Stochastic Environmental Research and Risk Assessment (2023) 37:1039–1052
https://doi.org/10.1007/s00477-022-02333-9

ORIGINAL PAPER

Models of bed-load transport across scales: turbulence signature from grain motion to sediment flux

Cristián Escauriaza[1] · Christian González[1,2] · Megan E. Williams[3] · Wernher Brevis[1,4]

Accepted: 25 October 2022 / Published online: 1 November 2022

Abstract

Sediment transport controls the evolution of river channels, playing a fundamental role in physical, ecological, and biogeochemical processes across a wide range of spatial and temporal scales on the Earth surface. However, developing predictive transport models from first principles and understanding scale interactions on sediment fluxes remain as formidable research challenges in fluvial systems. Here we simulate the smallest scales of transport using direct numerical simulations (DNS) to explore the dynamics of bed-load and discover how turbulence and grain-scale processes influence transport rates, showing that their interplay gives rise to a critical regime dominated by fluctuations that propagate across scales. These connections are represented using a stochastic differential equation, and a statistical description through a path integral formulation and Feynman diagrams, thus providing a framework that incorporates nonlinear and turbulence effects to model the dynamics of bed-load across scales.

Keywords Sediment transport · Numerical models turbulence

1 Introduction

How rivers change over time is shaped by complex nonlinear processes that take place at the interface of the sediment bed and the flow. In most cases, their morphodynamic evolution is controlled by sediment motion in close contact with the bed, or bed-load transport (Church 2006), which is originated at the smallest physical scales, driven by the dynamics of the turbulent boundary layer at the particle size. Sediments interact with recurring and self-sustained patterns of the flow velocity near the bed that reveal a wide range of organized eddies, predominantly streaks and hairpin vortices of different sizes (Adrian 2007; Smits et al. 2011; Marusic and Adrian 2013). These coherent vortices constitute the fundamental structure of the boundary layer, which very close to the bed produce spatially correlated velocity fluctuations influenced by viscosity, transferring momentum and mobilizing sediment grains downstream (Séchet and Le Guennec 1999; Radice et al. 2013; Cameron et al. 2020). Interactions of particles with the turbulent flow have a remarkable complexity and significant consequences on the channel morphology for a wide range of spatial and temporal scales. Even though the couplings and feedbacks that affect bed-load transport are not entirely known, quantitative studies of the

C. González, M. E. Williams, W. Brevis, contributed equally to this work.

✉ Cristián Escauriaza
cescauri@ing.puc.cl

Christian González
cgonzle1@asu.edu

Megan E. Williams
megan.williams@usm.cl

Wernher Brevis
wbrevis@ing.puc.cl

[1] Departamento de Ingeniería Hidráulica y Ambiental, Pontificia Universidad Católica de Chile, Av. Vicuña Mackenna 4860, 7820436 Macul, Santiago, Chile

[2] School of Geographical Sciences and Urban Planning, Arizona State University, Tempe, AZ 85287, USA

[3] Departamento de Obras Civiles, Universidad Técnica Federico Santa María, Av. España 1680, 2390123 Valparaíso, Chile

[4] Departamento de Ingeniería en Minería, Pontificia Universidad Católica de Chile, Av. Vicuña Mackenna 4860, 7820436 Macul, Santiago, Chile

morphodynamic evolution of river channels have always required models to predict transport rates, from the study of sediment relations with the scales of turbulence, to investigations on the effects of tectonic motions (Church 2007). However, modeling transport from first principles is a very difficult task, since different nonlinear processes and flow features that are important to predict sediment fluxes depend on the scale of observation, which also determines the variables used in the models to represent the system. At larger scales, the problem is further complicated as the dynamics of turbulence and bed-load transport give rise to emergent phenomena, producing self-organized patterns that evolve slowly, at spatial scales much larger than the grain advection lengthscales (Werner 1999; Murray et al. 2009; Ganti et al. 2014). These large-scale sedimentary structures, such as ripples, dunes or bars, also play an important role on flow resistance and on the evolution of the drainage network. In addition, these phenomena are related to multiple other interactions and feedbacks that can affect bed-load transport, including ecological and biogeochemical processes, as well as geological and anthropic factors (Pledger et al. 2014; Vignaga et al. 2013; Ravazzolo et al. 2019; Kirby and Whipple 2012; Wohl 2019; Yang and Nepf 2019).

The prediction of the sediment transport capacity for geological, geomorphological, or engineering applications has traditionally been carried out from a continuum/Eulerian perspective, abstracting an inherently discrete system comprised by many particles of different sizes and shapes that are mobilized by the flow, into a sediment transport flux expressed as the total volume of sediment per unit width per unit time in a channel cross-section (q_b [m^2/s]). Transport formulas for q_b are derived from field data or laboratory experiments in steady unidirectional flows, as a function of bulk parameters of the flow, and based on either Bagnold (1956) or Einstein (1937, 1950) hypotheses. These descriptions are mostly empirical, without an explicit definition of the scales involved in the model, as similar formulas are used to predict the initial stages of bedform development induced by turbulence (Escauriaza and Sotiropoulos 2011a; Khosronejad and Sotiropoulos 2014) or to define transport laws to simulate landscape evolution in the long-term (Barnhart et al. 2020). The fluxes obtained from these formulas typically overpredict the average magnitude of transport and they do not account for the intermittency that is observed in bed-load transport measurements (Frey and Church 2009). At larger spatial and temporal scales, evidence shows that intermittent transport rates arise from either internal autogenic processes (Paola 2016), or from the external forcing when the time-scales of the input signal are larger than the scales of autogenic variability (Jerolmack and Paola 2010). At the smallest scales, at which bed-load transport is originated, intermittency is driven by turbulent fluctuations and interactions with sediment particles, as shown in Fig. 1, producing frequent transport events of different magnitudes (Escauriaza and Sotiropoulos 2011b; González et al. 2017). Models aimed at predicting bed-load transport rates are therefore crucial to provide insights on the fundamental processes of sediment dynamics, how turbulence influences sediment motion, and the potential connections among scales to understand the scope of application (Escauriaza et al. 2017).

Here we propose two models to understand these connections: First we explore the physical mechanisms of interaction between turbulence and sediment motion at the smallest scales, with a model that can resolve the particle dynamics coupled with the turbulent boundary layer flow (González et al. 2017). We then pursue a model integration (Escauriaza et al. 2017), using statistical information of the high-fidelity approach to inform a larger scale stochastic one-dimensional (1D) model for the bed-load transport rate. We compute the flux from the viewpoint of an external observer of the system to answer two important questions: (1) Does the small-scale mechanics of sediment motion have an influence on the flux observed at larger scales? (Furbish et al. 2012; Heyman et al. 2013; Ancey and Pascal 2020); and (2) Can we improve the prediction of bed-load transport formulas using high-resolution simulations? Intuitively, the answer to the these questions is that temporal and spatial averaging swiftly erase the turbulence signature, and that small-scale processes do not contribute to the observed transport rates. However, in our simulations we observe the emergence of a critical regime, at which transport fluctuations are propagated across scales.

The advantages of implementing stochastic equations in sediment transport have been demonstrated since the pioneering work of Man and Tsai (2007), who developed a model to represent particle trajectories and suspended load concentrations, considering the turbulence effects in the random term. Recent developments of these methods show that the effects of turbulence fluctuations can be captured on particle statistics, generating probability distributions of suspended sediment fluxes observed at larger scales, and they can reveal additional details of particle dynamics (Tsai et al. 2018; Oh and Tsai 2018; Tsai et al. 2020) and incorporate the sediment size distributions (Huang et al. 2021). In bed-load transport we assume here that a simple 1D stochastic model can represent fluctuating transport for uniform sediment, and reproduce the intermittency observed in fluxes of high-fidelity numerical simulations.

In this work we discuss the physical basis of these fluctuations that appear in bed-load at larger scales and we connect the two modeling approaches at different scales to capture the transport dynamics and find analytical

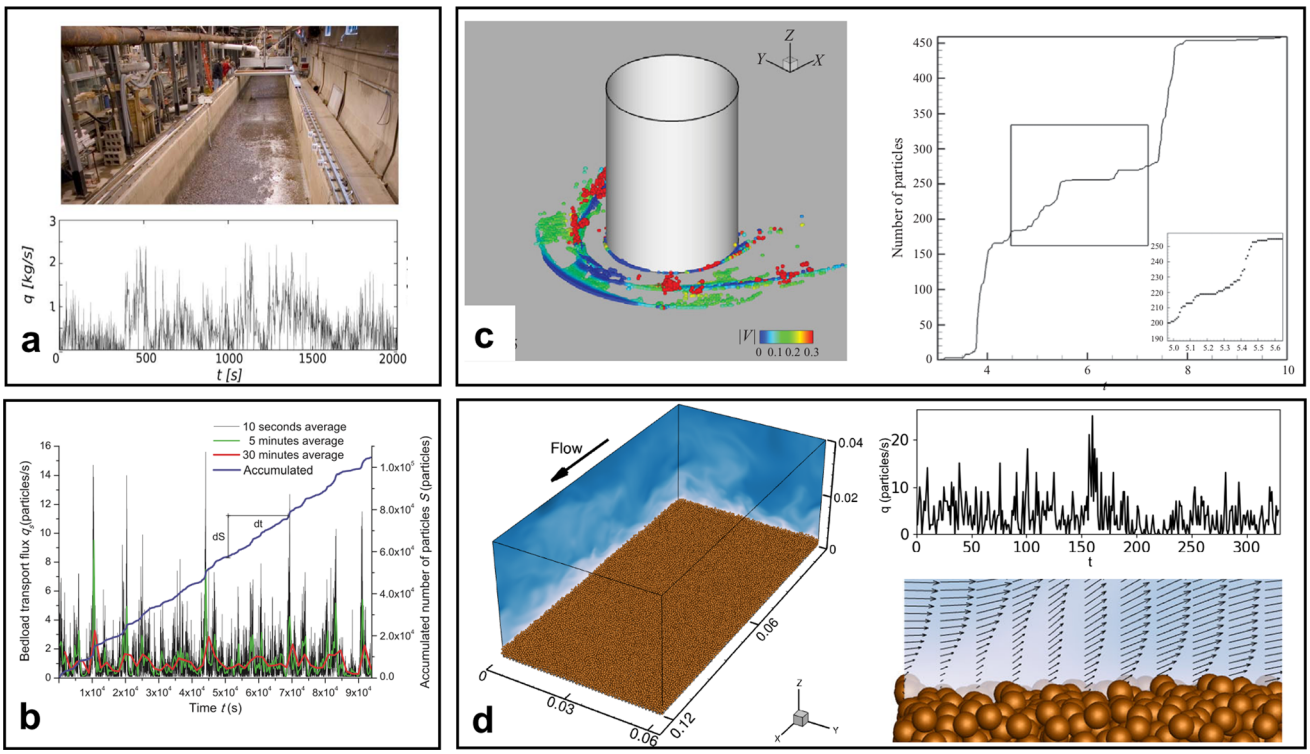

Fig. 1 Fluctuations in bed-load transport fluxes emerges at time and lengthscales much larger than the scales of particle motion. **a** Bed-load transport data from experiments (Jerolmack and Paola 2010). **b** Experimental time-series of bed-load observed at different time scales for high flow velocities by Ma et al. (2014). **c** Numerical simulations of intermittent bed-load transport by the turbulent horseshoe vortex system generates a cumulative sediment transport represented by a self-similar devil's staircase fractal distribution (Escauriaza and Sotiropoulos 2011b). **d** Computational domain, instantaneous near-bed flow, and bed-load transport flux, from the model of González et al. (2017) used in this investigation

expressions for the statistical moments of transport using renormalized perturbation expansions from a stochastic action, summarized as a superposition of Feynman diagrams. The results underscore the role of the smallest scales of particle motion and turbulence on the transport rates, and the implications on modeling bed-load by connecting approaches at different scales.

2 Critical transport driven by collective motion

Particle models correspond to the maximum level of physical fidelity and space-time resolution of sediment motion. To study bed-load transport at these small scales, we model the dynamics of each individual particle and the momentum interactions with the flow field and with other particles in motion or in the bed. Lagrangian approaches consider the sediment transport processes from a granular perspective (Frey and Church 2009; Schmeeckle 2014; Houssais et al. 2015; Ferdowsi et al. 2017) by integrating the trajectory and momentum equations of each particle, and accounting for particle–particle interactions and the effects of the instantaneous forces produced by the turbulent flow. The Navier–Stokes equations are solved using direct numerical simulations (DNS), resolving all the scales of turbulence with a grid resolution of the same order of magnitude as the Kolmogorov scale, the smallest scale of the system at which viscosity dissipates kinetic energy. The discrete-element model (DEM) is used for sediment particles (Schmeeckle 2014), which computes collisions between grains using a point-particle approach, assuming particles as spheres. The computational domain and details of the instantaneous flow field near the bed are shown in Fig. 1d. The simulations of González et al. (2017) are employed here with the computation of two additional cases as numerical experiments to analyze the time series of bed-load transport.

The DNS-DEM model is based on the coupled solution of the Navier–Stokes (N-S) equations, and the momentum and trajectory equation for each particle. The incompressible N-S equation for mass and momentum conservation in Cartesian coordinates can be written in tensor notation as follows,

$$\frac{\partial u_j}{\partial x_j} = 0 \tag{1}$$

$$\rho\left(\frac{\partial u_i}{\partial t} + u_j\frac{\partial u_i}{\partial x_j}\right) = -\frac{\partial p}{\partial x_i} + \mu\frac{\partial^2 u_i}{\partial x_j \partial x_j} + F_i \tag{2}$$

where u_i are the velocity components, p is the pressure, ρ is the fluid density, μ the viscosity, and F_i is the forces of the particles acting on the fluid. The governing equations for the position and velocity of each particle read in tensor form as:

$$\frac{dx_i}{dt} = v_i \tag{3}$$

$$m\frac{dv_i}{dt} = f_i \tag{4}$$

where m is the particle mass, and x_i and v_i are the particle location and velocity, respectively. The hydrodynamic forces, gravity, and collisions are included in the vector f_i (Escauriaza and Sotiropoulos 2009). The set of equations are integrated using a third-order Runge–Kutta scheme, using a sixth-order Lagrange interpolation to obtain the flow velocities at the particle locations. The particle Reynolds number is maintained constant ($Re_* = \rho u_* d/\mu = 7.0$) by modifying the sediment density, and the Shields parameter is varied. In the definition of Re_*, the length scale is the particle diameter d. For details of the model and parameters used in the simulations the reader is referred to González et al. (2017).

We perform simulations to capture the details of sediment motion that are driven by the turbulent motions of the boundary layer, and characterize the system using the non-dimensional Shields parameter τ_*, defined as follows,

$$\tau_* = \frac{\tau_0}{(\rho_s - \rho)gd} \tag{5}$$

where τ_0 is the mean bed shear stress of the flow, ρ_s and ρ are the sediment and water density, respectively, g is the acceleration of gravity, and d is the particle diameter.

We consider six simulations (González et al. 2017) using a constant particle diameter, and maintaining the Reynolds number of the bulk flow and the particle Reynolds number constant by changing the sediment density, to retain the statistical properties of the forcing exerted by turbulence on sediment grains. These high-resolution numerical simulations are employed to study the evolution of bed-load transport flux from an Eulerian standpoint as an external observer, quantifying the number of particles that cross a vertical plane perpendicular to the streamflow direction, and dividing the total mass by the measurement time. The transport rate is computed after the coupled system statistically converges, performing a long simulation period. After this initial convergence, the data is then collected, and the averaged non-dimensional bed-load flux for each Shields parameter is obtained (This procedure is the same as established in González et al. 2017) (Fig. 2). This "measurement" of bed-load transport is equivalent to the output yielded by formulas commonly used for predicting the non-dimensional transport rate, which are based on dimensional analysis and experimental or field data. The non-dimensional transport q_* is defined as follows,

$$q_* = \frac{q_b}{\sqrt{(s-1)gd}} \tag{6}$$

where $s = \rho_s/\rho$ is the sediment specific gravity. The DNS results agree well with the common scaling of q_* with respect to the Shields parameter τ_*, which exhibits an exponent equal to 3/2, shown as a solid line in the plot (Fig. 2a).

The scaling of bed-load transport rate with the Shields parameter across an order of magnitude with a constant exponent for the convergent cases is due to the dynamic similarity of the flux with the Shields number, which predicts a stable convergence of the averaged number of particles passing through a cross section per unit time. However, two cases stand out from the plot that generate a smaller average flux compared to the 3/2 law. When we examine these cases that are overpredicted by the analytical formula, we observe that the dynamics does not converge smoothly to the average, but exhibit large-scale fluctuations that seem to be bounded in amplitude but are significantly larger than the mean. To compare the changes on the dynamics of the system as a function of τ_*, we show three cases of the standardized series of bed-load flux to show the convergence on small and large values of the Shields parameter to the average, while the intermediate case ($\tau_* = 0.08$) is dominated by large fluctuations with respect to the mean (Fig. 2b). The fluctuating cases exhibit a significant standard deviation that also implies a large coefficient of variation, which will require a stochastic approach.

The non-dimensional parameter τ_* that represents the relation between the averaged turbulent stresses and gravity, can be used to quantify the leading mechanism of bed-load transport variability: For a small value of the Shields number, transport is sustained but the system is dominated by gravity and it is very slow to react to turbulent stresses. As the Shields number increases, however, turbulence has a more predominant role and instantaneous localized events of intense stresses on the bed mobilize groups of particles at different locations (Fig. 3), producing a striking transport regime characterized by bed-load transport bursts leading to a persistence of fluctuations in the global flux. This regime is characterized by collective motion, defined as the simultaneous entrainment of a group of particles lying closely on the bed by the effect of turbulent stresses.

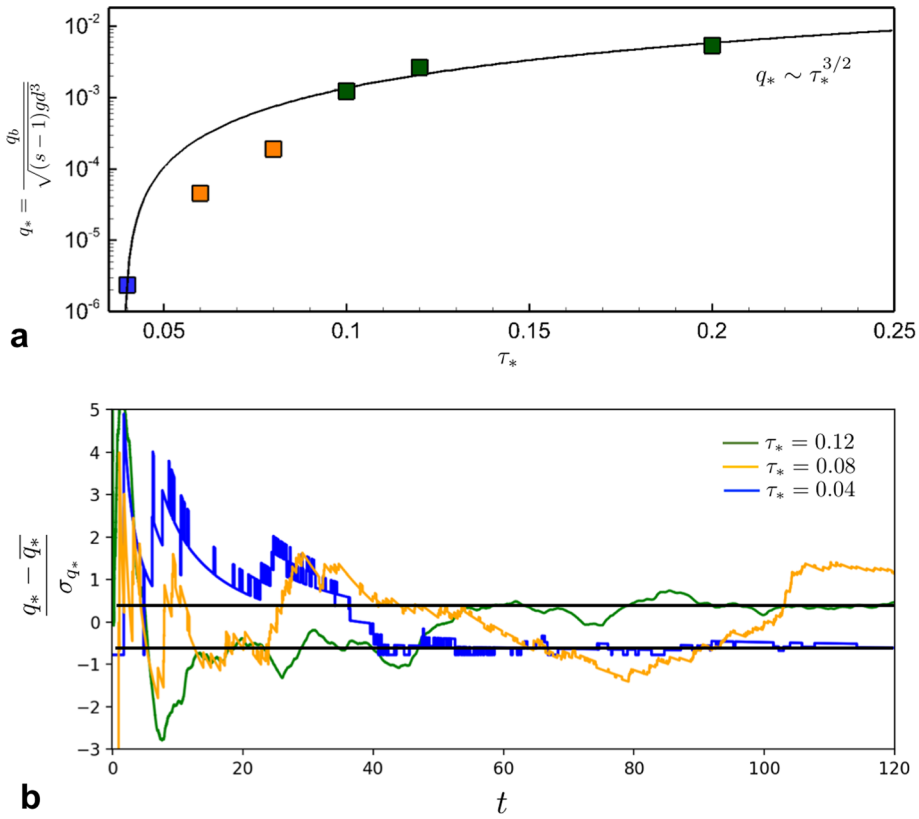

Fig. 2 Bed-load transport flux from the Lagrangian model. **a** Averaged bed-load transport rate computed from DNS, the continuous line corresponds to a fit to an analytical equation with exponent 3/2. **b** Standardized time-series of the system shows examples of convergence to almost constant values of the time average for the smallest Shields number case and for one of the largest cases (black lines are converged averages), and the fluctuating dynamics of transport exhibited by the cases overpredicted by the formula

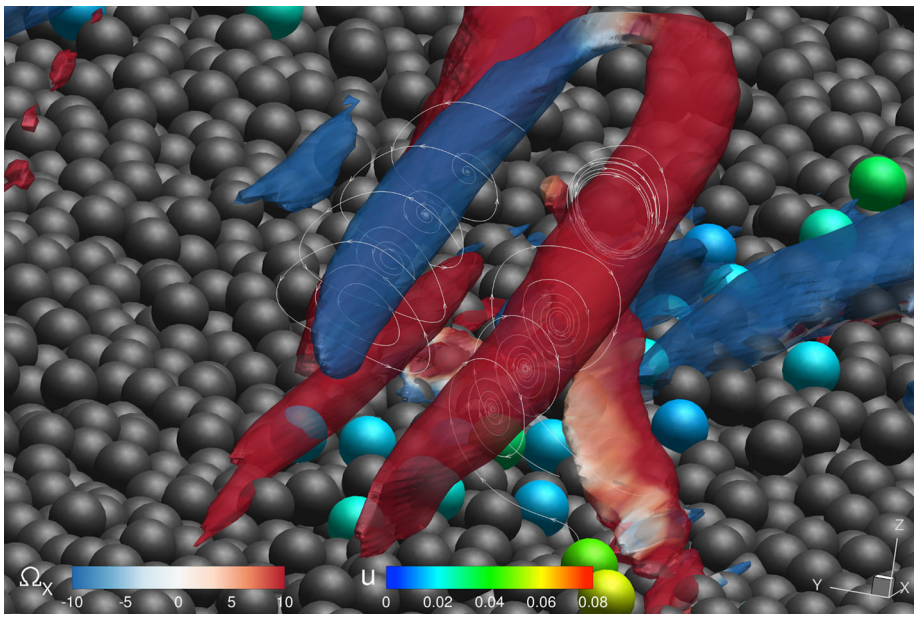

Fig. 3 Collective particle motion. An instantaneous image shows a vortical structure of the turbulent boundary layer known as a hairpin vortex, visualized with the q-criterion (Hunt et al. 1988), colored by vorticity in the streamwise direction. Sediments are colored by their velocity magnitude, as a sweep event mobilizes a group of particles

For larger values of τ_*, the collective transport of particles becomes widespread on the entire bed surface, the flux is fully dominated by turbulence and the relative magnitude of the fluctuations becomes smaller compared to the mean transport rate. In this high τ_* regime, collective motion occurs continuously on the entire surface of the bed, and the system responds quickly to the flow but independent transport events become invisible in the statistical moments of transport. The dynamic equilibrium conditions are therefore controlled by the stress-gravity balance: In low transport flows, the temporal and spatial variability of turbulent stresses are stabilized by gravity and the system converges to the mean value of transport. This intermediate state of transport is produced by the unstable balance

between gravity and turbulent stresses that is reflected in the Shields parameter. The emergence of this critical regime breaks the scale-invariance of transport, and affects the mean and higher-order moments, producing a fluctuating signal at larger scales.

3 Stochastic nonlinear model and bed-load transport statistics

In the critical regime the large-scales of transport are connected to the collective motion of the grains, as the small-scale intermittent events on the bed generate a bed-load flux that exhibits fluctuations of transport at time and length scales larger than the particle dynamics. These episodic transport conditions produce a non-stationary response of the entire system, which can no longer be represented by a deterministic bed-load function. The complex dynamics of grains associated to the collective transport events yields a large-scale dynamics that appears stochastic from a global perspective.

To improve our predictions of bed-load transport we develop a model at a higher-level of abstraction based on the data obtained from the Lagrangian DNS model. We consider a dynamical system that comprises the entire computational domain from an Eulerian perspective, considering the evolution of the sediment transport rate in a cross section as the global response, at spatial and temporal levels outside the particle scale processes. A simple model to reproduce the fluctuations in the bed-load flux considers the domain as a control volume where we apply the momentum balance for the sediment from an integral perspective, which averages the details of grain-scale interactions. This spatial integration filters the intrinsic variability and unsteady distributions of collective transport events produced by turbulent stresses, and the effects of particle collisions on the flux.

We consider the computational domain in Fig. 1d as a control volume to derive a global equation of transport for the entire domain. The integral momentum equation can be written in vector form as:

$$\frac{\partial}{\partial t}\int_{\forall_c}\rho_s\overrightarrow{\mathbf{V}}d\forall+\int_{S_c}\rho_s\overrightarrow{\mathbf{V}}\left(\overrightarrow{\mathbf{V}}\cdot\hat{\mathbf{n}}\right)dA=\sum\overrightarrow{\mathbf{F}} \tag{7}$$

where $\overrightarrow{\mathbf{V}}$ is the sediment velocity integrated in the entire domain or control volume ($\forall_c$), enclosed by the control surface (S_c). From this relation we can derive a simple nonlinear model of transport evolution: We consider the bed-load transport to be one-dimensional, and the periodic boundaries of the domain cancel the integral of the flux across the control surface. Assuming spatial uniformity of the domain, the statistics of the transport flux have the same properties in all cross-sections, and the 1D momentum equation derived from Eq. (7) can be expressed as follows:

$$\rho_s\frac{dq_b}{dt}=f_{internal}+f_{forcing} \tag{8}$$

where $f_{internal}$ and $f_{forcing}$ are the 1D components of the integral forces per unit volume derived from the right hand side of Eq. (7). This equation shows that a force imbalance between the internal bed dynamics and the hydrodynamic forcing integrated in space is a source of bed-load flux, producing a variation in time of q_b. The first term in the right hand side represent the nonlinear internal interactions of the particles that generates a dynamic dependence of the bed-load flux. The second term $f_{forcing}$ represents the external forcing acting on the bed, i.e. the stresses exerted by the coherent structures of the turbulent boundary layer that are relevant for the particles.

The simplest formulation to represent the nonlinear dynamics of the system $f_{internal}$, as the bed experiences changes due to bed-load transport (Masteller and Finnegan 2017), is a quadratic function. This expression can also be thought of as a second-order Taylor expansion to represent the nonlinear internal dependence. The external input corresponds to the combined instantaneous hydrodynamic forces acting on the entire domain seen at large scales. This input is assumed as a white noise in the definition of the stochastic differential equation, which corresponds to the derivative of a Wiener process (Bressloff 2014; Chow and Buice 2015).

From this analysis we propose a stochastic differential equation with additive noise (Gardiner 2009; Särkkä and Solin 2019) that represents the temporal evolution of the flux as a consequence of the imbalances between the driving and resistive forces integrated in the control volume. Instead of considering the evolution of bed-load transport as a linear process, we explicitly adopt a nonlinear formulation, since sediment motion changes the local flow conditions and modifies the exposure of grains, which in turn changes the entrainment of particles and their transport (Masteller and Finnegan 2017). The model incorporates the simplest nonlinear parameterization of the internal dynamics in the deterministic part of the stochastic equation to represent the internal mechanisms of the bed at work. This is a global spatial equation for the evolution of the bed-load transport flux in time, in which the deterministic part of the model is a basic nonlinear approximation for the entire computational domain, with a random input forcing process. The nonlinear stochastic version of the momentum Eq. (8) can therefore be written in nondimensional form as follows,

$$dq_*=\left(-aq_*+bq_*^2\right)dt+\sqrt{D}\,dW \tag{9}$$

where q_* is the non-dimensional bed-load transport flux, the internal nonlinear dynamics of the system contains the parameters a and b, and the random input dW is the increment of a Wiener process (Man and Tsai 2007; Gardiner 2009) scaled with the dispersion coefficient D. These parameters are obtained by using maximum likelihood with an extended Kalman filter (Kristensen and Madsen 2003; Kristensen et al. 2004), using the DNS-DEM data (see Table 1).

It is important to emphasize that linear stochastic approaches have already been used to represent specific features of transport, based on Langevin-type of equations for particle velocities (Fan et al. 2016; Tsai and Huang 2019) or master equations that reproduce the evolution bed-load transport rate or the distribution of moving particles on the bed (Furbish et al. 2012; Ma et al. 2014; Ancey et al. 2015). For this large-scale model we derive a stochastic expression from the momentum balance equation of the domain that represents the emergence of the transport signal at scales significantly larger than the particle step lengths. The model can be solved numerically (Rößler 2010; Särkkä and Solin 2019) to produce synthetic series of bed-load transport rate statistically indistinguishable from the DNS model to compute histograms of transport.

We can further simplify the analysis of these complex conditions, deriving analytical expressions for bed-load statistics based on the probability distribution function (PDF) of different realizations of the transport rate, as represented by the large-scale stochastic model. As proposed by Chow and Buice (2015) (see also Bressloff 2014), the PDF of the flux is expressed as follows,

$$P[q_*(t) \mid q_*(0)] = \int e^{-S[q_*(t),\tilde{q}_*(t)]}\, \mathcal{D}\tilde{q}_*(t) \tag{10}$$

where $S[q_*(t), \tilde{q}_*(t)]$ is the stochastic action of the system or Onsager–Machlup functional, $\tilde{q}_*(t)$ is a complex wavenumber function, and $\mathcal{D}\tilde{q}_*(t)$ indicates that we perform a functional integration on realizations of the process. This is known as the path-integral formulation (Feynman and Hibbs 1965) or Wiener integral (Gardiner 2009; Bressloff 2014) of the dynamical system to define the PDF. Equation (10) can be interpreted as an integration over all the possible realizations that the transport process can experience, which depends on the stochastic action of the dynamical system in Eq. (9). This is equivalent to the principle of stationary action in classical mechanics, in which bed-load transport series with the smallest action (S), have a larger contribution to the probability distribution ($\sim e^{-S}$).

Table 1 Coefficients of the nonlinear stochastic bed-load transport models for the critical regime

	$\tau_* = 0.06$	$\tau_* = 0.08$
a	7.66×10^{-2}	3.75×10^{-2}
b	5.65×10^{-4}	7.10×10^{-3}
$\sqrt{D}$	1.00×10^{-5}	1.00×10^{-5}

The methodology to approximate analytically the moments of the nonlinear equation is based on the definition of the characteristic functional, also known as the moment generating functional:

$$Z[J,\tilde{J}] = \int e^{-S[q_*(t),\tilde{q}_*(t)] + \int \tilde{J}(t) q_*(t) dt + \int J(t)\tilde{q}_*(t) dt} \times \mathcal{D}q_*(t)\mathcal{D}\tilde{q}_*(t) \tag{11}$$

or the cumulant generating functional $W[J,\tilde{J}] = \ln Z[J,\tilde{J}]$, where all the moments are obtained by performing functional derivatives of Z or W in terms of the complex source functions $J(t)$ and $\tilde{J}(t)$ (Buice and Cowan 2007; Chow and Buice 2015; Lera 2018). Since this integral can only be calculated analytically for the first order linear equation, we approximate the moment of bed-load transport by separating the action in Eq. (11) into the linear or free part (S_F), and the so-called interacting part (S_I) that contains the small nonlinear term and stochastic input (Buice and Cowan 2007), $S = S_F + S_I$, as follows:

$$\begin{aligned} Z[J,\tilde{J}] &= \int e^{-S_F - S_I + \int \tilde{J} q_* dt + \int J \tilde{q}_* dt}\, \mathcal{D}q_*(t)\mathcal{D}\tilde{q}_*(t) \\ &= \int e^{-S_F} \sum_{n=0}^{\infty} \frac{1}{n!} \left(-S_I + \int \tilde{J} q_* dt + \int J \tilde{q}_* dt \right)^n \\ &\quad \times \mathcal{D}q_*(t)\mathcal{D}\tilde{q}_*(t) \end{aligned} \tag{12}$$

Taking the integral within the sum, the characteristic functional is expanded as a series of free moments of the interacting part. The solution of the linear part from S_F corresponds to the impulse response function of a first-order differential equation, also known as the propagator or Green function $G(t,t') = e^{-a(t-t')}$ for $t > t'$. The generating functionals Z and W for the nonlinear stochastic equation are then expanded in terms of $G(t,t')$, using a perturbative expansion of the exponential of S_I around the free action. From the Itō condition for the temporal dependence of the process (Gardiner 2009) and Wick's theorem (Chow and Buice 2015), we preserve only the non-zero free moments with the same number of $q_*(t)$ and $\tilde{q}_*(t)$.

The derivation of the sum of terms of the expansion in Eq. (12), however, becomes rapidly unmanageable and difficult to follow (Chow and Buice 2015). To simplify the analysis, we express the moments of bed-load transport as a sum of Feynman diagrams, defining rules to draw the terms

having the largest contributions in the expansion. Each interacting term of the series represents external vertices of the diagram, with ingoing and outgoing edges for each q_* and $\tilde{q}_*$ field, respectively. These vertices are connected by straight arrows, which correspond to the propagators $G(t_2, t_1)$ for $t_2 > t_1$, flowing in time from left to right (see Appendix A). Using Wick's theorem and the Itō convention, only fully connected diagrams survive in the expansion of cumulants, and they are multiplied by symmetry factors of repeated diagrams in the series (Chow and Buice 2015). It is important to note that stochastic diagrammatic expansions have been already been employed in environmental flows to determine hydraulic conductivity in porous media, obtaining distributions of effective permeability in heterogeneous systems that present spatial fluctuations of local permeability (Hristopulos and Christakos 1999).

The diagrams used here are composed from building blocks that represent the terms of the interacting action shown in Eq. (12) (see Appendix A). Therefore, the mean of bed-load transport computed with a third-order expansion for q_*, from the stochastic model is obtained as follows:

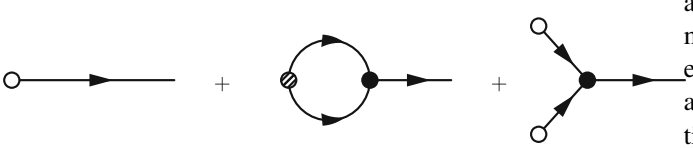

(13)

This expression yields the approximation of the average as a function of the propagator, which including an initial condition of the system q_{*0}, is equal to:

$$\begin{aligned}\overline{q}_*(t) &= q_{*0}\, G(t,t_0) + bD \int G(t,t_1) G^2(t_1,t_2) dt_1 dt_2 \\ &\quad + bq_{*0}^2 \int G^2(t_0,t_1) G(t,t_1) dt_1 \\ &= q_{*0} e^{-a(t-t_0)} + \frac{bD}{2a^2}\left[1 - e^{-a(t-t_0)}\right]^2 \\ &\quad + \frac{bq_{*0}^2}{a}\left[e^{-a(t-t_0)} - e^{-2a(t-t_0)}\right]^2\end{aligned} \tag{14}$$

As $t \to \infty$, the first moment of bed-load transport converges to an analytical expression obtained from the coefficients of the stochastic transport model:

$$\overline{q}_* = \frac{bD}{2a^2} \tag{15}$$

Following the same approach, the third-order diagrammatic expansions of the cumulant generating functional to obtain the variance and skewness of the transport flux from the cumulant generating functional can be expressed as follows:

(16)

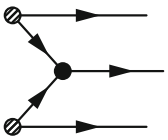

(17)

These approximations converge to equations for the moments of bed-load transport that can be calculated analytically, which converge to the following expressions:

$$\sigma_{q_*}^2 = \frac{D}{2a} \tag{18}$$

$$\gamma_{q_*} = \frac{b\sqrt{2D}}{3a^{3/2}} \tag{19}$$

The moments derived from these diagrammatic expansions represent the statistics of transport in the critical regime, and predict accurately the results from the Lagrangian model coupled to DNS for the non-convergent conditions, except for the initial variability that affects the skewness, as shown in Table 2. This analytical large-scale formulation is based on the stochastic dynamics, when the random input and the nonlinearity are explicitly considered as part of the system and used to approximate the statistics of the fluctuating flux in the critical regime.

4 Discussions and conclusions

The emergence of fluctuations in bed-load fluxes has been recognized as major a feature of transport in experiments and field observations. As shown here by the high-fidelity DNS model, collective particle motion driven by turbulence is the leading mechanism that produces the fluctuating regime in the studied domain. This mode of transport was first identified in the field by Drake et al. (1988), who reported frequent localized transport events and described brief episodes of collective particle motion in a series of intermittent displacements, occurring due to turbulent fluctuations of the boundary layer. Experimental evidence has also shown that hydrodynamic forces play a fundamental role on bed-load dynamics, in which sweep events of the boundary layer generate the transport events (Radice et al. 2013), although collective motion also arises in near-threshold conditions on steep slopes (Heyman et al. 2013) or in cases without the direct influence of turbulent stresses, when fluctuations are driven by collisions or by slow

Table 2 Moments of bed-load transport in the critical regime obtained from DNS and from the renormalized perturbation expansion using Feynman diagrams

	$\tau_* = 0.06$		$\tau_* = 0.08$	
	DNS	Renormalization	DNS	Renormalization
$\overline{q}_*$	5.9588×10^{-5}	5.9588×10^{-5}	1.9568×10^{-4}	1.9568×10^{-4}
σ_{q_*}	2.5545×10^{-5}	2.5548×10^{-5}	3.6507×10^{-5}	3.6514×10^{-5}
γ_{q_*}	4.37	0.095	−0.89	−0.1

subsurface creeping of the granular material in the bed (Houssais et al. 2015; Lee and Jerolmack 2018).

Through DNS we observe that in a uniform sediment bed, the Shields parameter can be used to identify the emergence of a critical regime, driven by the dynamic competition of resistive forces and turbulent stresses that strengthen the collective motion process, and produce fluctuations on the integrated flux for the entire computational domain. We believe that this critical regime is the same that was reported by Gilbert (1914), who observed a transition in bed-load characterized by collective motion and "rhythmic" transport, sequences of events in which groups of particles were continuously mobilized.

To provide an answer to the first question we posed initially: The small-scale dynamics of sediment motion is observed in the large-scale flux when the collective motion is activated. As the turbulent stresses increase with respect to the gravitational and resistive forces, the cumulative effect of the coherent structures of the boundary layer are imprinted on the spatial and temporal averages, from which we compute the bed-load transport rates. Therefore, local particle interactions in a spatially distributed system become relevant, and the turbulence signature appears in the bed-load transport rate for intermediate Shields numbers. As turbulent stresses increase, the mechanisms that produce fluctuations are still present, but they do not compare in magnitude to the average transport, and the bed-load flux converges as the system reaches a dynamic equilibrium that can be represented by the power law relation. The critical window that breaks the scaling relation emerges by the competition of forces acting on the bed. These results indicate that in addition to the kinematic scaling used to identify allogenic signals on the response of sedimentary signals (Jerolmack and Paola 2010; Ganti et al. 2014), the turbulence signature observed on the bed-load flux shows the relevance of observing the dynamic scaling, expressed here as the relation between flow stresses and resistive forces in the Shields parameter.

The critical regime of bed-load transport connects the small-scale dynamics of the particles to the larger-scale measurements of the flux, which are typically made with no access of the processes at the grain level. The changes with the Shields parameter resemble the critical phenomena and equilibrium phase transitions that are observed in multiple physical systems, which constitute one of the fundamental subjects of statistical mechanics and field theory (Sornette 2006; Herbut 2007). In our case the system goes through a transition for the range of Shields numbers that reflects an equivalent influence of turbulent stresses and resistant forces. Collective transport events in this regime generate regions of spatial correlation on the bed surface, or islands of motion that exist for a brief period of time. Therefore, the continuous appearance of particle groups moving intermittently produces time intervals when the averaged bed-load flux grows significantly, followed by periods of low transport. These changes produce a fluctuating time series, with an average that departs from the other cases, breaking the scale invariance of the system represented by a constant exponent.

This analogy with critical phenomena in other physical systems suggests that we should base our bed-load transport analysis on statistical field theory and techniques that provide approximations of macroscopic large-scale observations of a system composed of multiple interacting elements. As a strategy to account for scale interactions and collective transport, the system is suitable to apply renormalization group transformations (McComb 2004; Sornette 2006), which will be explored in the future to describe the scaling laws considering the effects of the fluctuations on the critical regime. As an example, we test the generalized complex exponent in the power-law between the parameters q_* and τ_* to incorporate the effects of fluctuations as a correction that introduces log-periodic oscillations in this relationship (Saleur et al. 1996; Sornette 2006). In Fig. 4, we show that this exponent provides a good representation of the averaged flux, which considers the effects of the fluctuations on the self-similar structure of bed-load transport for the range of Shields parameters. In the critical regime, the exponent for the average seems to be smaller than 3/2, while for lower values of τ_* is high (Shih and Diplas 2018). It is important to consider that the simulations studied in this investigation are based on an idealized domain with a uniform sediment size, but the strategy of connecting models at different scales by using stochastic techniques that incorporate explicitly the nonlinearity of

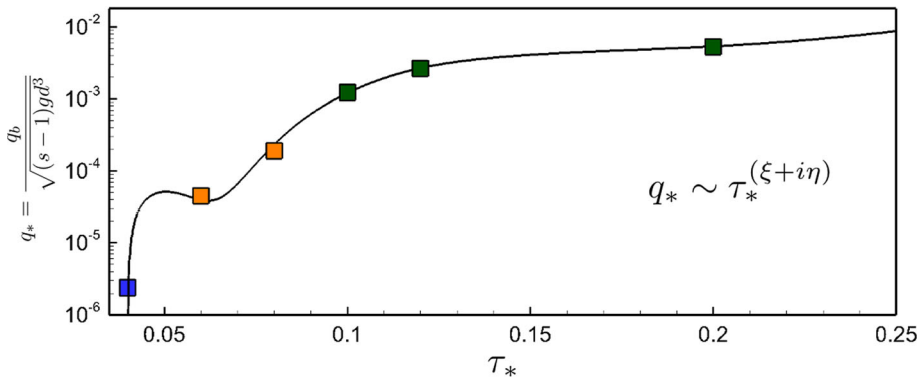

Fig. 4 Generalized exponent for the averaged bed-load transport flux. Assuming that the power-law relationship between the averaged bed-load transport flux and the Shields parameter is a scaling law for the range of DNS simulations, we correct the exponent to consider the effects of fluctuations as log-periodic oscillations using a complex number exponent, as proposed by Saleur et al. (1996)

the process provides a pathway to incorporate additional and more realistic effects in the near future.

On the other hand, the 1D stochastic model that represents the bed-load flux on the entire domain provides an answer to our second question, by incorporating the fluctuating dynamics originated by the interactions of the particles with turbulence as a nonlinear dynamical system. We propose a predictive bed-load transport model that captures the complexity of the flux observed in the Lagrangian DNS approach at a larger scale, considering explicitly the nonlinear dependence of q_* and representing the integrated turbulent forcing as a random process with parameters obtained from the results of the high-fidelity simulations. The system reproduces the dynamics of the critical bed-load transport regime that emerges at scales much larger that the turbulent transport events, without resolving the small-scale interactions or details of the particle motion.

The parameters of the stochastic dynamical equation reflect the memory of the system, nonlinearity, and relevance of the random input on the bed-load transport rate. Compared to long-established deterministic equations that have been successfully employed in a wide range of problems to predict the average transport capacity, the stochastic model can help us understand the physical mechanisms that control the evolution of bed-load transport by the changes of its parameters with the Shields number. The expansions using Feynman diagrams also provide simple analytical expressions for the moments of bed-load transport, as other recent advanced statistical formulations (Furbish et al. 2012; Ancey and Pascal 2020), but incorporating explicitly the fluctuations and nonlinearity of transport, and accounting for the variability of the flux under critical conditions, when fluctuations that are comparable to the mean dominate the transport signal. In this investigation we contribute to understand the relation between transport and turbulent stresses, connecting models at different scales by using a stochastic technique that incorporate explicitly the nonlinearity of the process, to advance toward more general predictions of the statistical moments of bed-load transport

Further modeling developments will be required to take full advantage of physically-based stochastic models, and to provide insights on bed-load transport mechanics from these approaches, beyond application purposes. In the studied domain we limited the analysis to the changes on the transport dynamics only as a function of the Shields number. The development of broader stochastic formulations will need a comprehensive definition of parameters that represent the controlling mechanisms acting on the system, to explore systematically their phase-space and identify the forces and internal bed processes that are relevant at different spatial and temporal scales. We anticipate that integrated models can be used to tackle more complex problems related to the dynamics of bed-load transport and to identify the origin of transport fluctuations at larger scales. Contributions of the nonlinear function and noise would vary as additional factors are incorporated in general conditions, for example as a consequence of sediment size distributions, as grains organise creating clusters and microforms (Hassan and Reid 1990), armoring (Bertin and Friedrich 2018), or interact with larger immobile particles (Ghilardi et al. 2014; Papanicolaou et al. 2018) that produce large fluctuations on transport rates. Processes of particle burial (Pierce and Hassan 2020), and sediment accumulation, storage and release (Paola 2016) that appear at larger spatial scales contribute to generate autogenic variability of transport, which emerges by grain interactions and nonlinear feedbacks.

Connecting high-resolution models with larger-scale formulations can also be designed to study transitions as the nonlinearity of the bed evolves, and the local interactions explain more complex global behavior. The emergence of bedforms and sedimentary patterns push the systems to new equilibrium conditions, generating interdependence between transport and near-bed turbulence (Leary and Schmeeckle 2017). Coherent structures, vortex interactions and flow separation induced by the growth and migration of bedforms modify turbulent stresses and

control bed-load transport fluctuations, introducing additional length and timescales (Guala et al. 2014), and a strong autogenic component on the response of the system. High-resolution numerical simulations have shown that incorporating the unsteady turbulent stresses in bed-load transport formulas is required to resolve the interactions that trigger the formation and evolution of sand ripples (Escauriaza and Sotiropoulos 2011a; Khosronejad and Sotiropoulos 2014), which underscores the need for reexamining predictive large-scale models of transport in the presence of transitions and emergent sedimentary patterns, since turbulent forcing is strongly modulated by the dynamics of bed-load transport. Stochastic approaches aimed at estimating the mean and the variability of transport would therefore need to introduce this dependence as a multiplicative noise in the equations (Särkkä and Solin 2019).

If there is hope on developing bed-load transport models based on physical principles that can combine deterministic representations of internal bed processes with the random dynamic contributions of the turbulent forcing and sediment variability, we will need to advance closely with experiments and field observations to discover the essential processes that can describe the sediment dynamics, and the aspects of the small scales that dominate or can be removed from predictive equations. Blending modeling techniques and using detailed data to parameterize high-level equations can help us understand the connections among scales, the changes of the systems as functions of these parameters, and the physical influences on other processes that take place on river beds.

Diagrams for approximating moments

The diagrammatic expansion is used to simplify the calculation of moments of bed-load transport from the first terms of Eq. (12), which corresponds to a sum of "free" moments based on the PDF of the free action, e^{-S_F}. Here we follow the procedure outlined by Chow and Buice (2015), defining a set of rules to draw the diagrams that represent each term in the expansion. The moments are obtained by integrating the functions with respect to the free action, and expressing them in terms of the propagator or Green function of the linear first-order equation $G(t_2,t_1) = e^{-a(t_2-t_1)} = \langle q_*(t_1)\tilde{q}_*(t_2)\rangle_F$ for $t_2 > t_1$, represented as an arrow in time, going from left to right. From Wick's theorem (Chow and Buice 2015) and the symmetry of Gaussian processes, all the odd-numbered free-moments are zero, and the even moments are expressed as the sum of the moments of all the possible pairings of the variables at different instants in time. The Itō interpretation (Gardiner 2009; Särkkä and Solin 2019) or causality of the stochastic system, ensures that the variables of the model only depend on the past. Therefore, each time integral of the expansion in the interacting part of Eq. (12) is represented by a vertex in each diagram, with incoming arrows for each q_* field, and outgoing arrows for each $\tilde{q}_*$ field. In this case we adopt the formulation and rules defined by Lera (2018), such that the diagrams that contain the initial condition (starting from a constant $\tilde{q}_{*0}$ value), the noise, and the nonlinear term are the following:

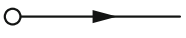

$$q_{*0}\tilde{q}_{*0} \tag{A1}$$

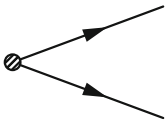

$$\frac{D}{2}\tilde{q}_*^2 \tag{A2}$$

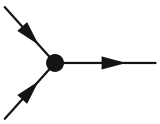

$$bq_*^2\tilde{q}_* \tag{A3}$$

These basic diagrams are the building blocks that are assembled to construct the expansion terms. Any general moment derived from the characteristic functional $Z[J,\tilde{J}]$ is defined as follows:

$$\left\langle \prod_{i=1}^{m}\prod_{j=1}^{n} q_*(t_i)\tilde{q}_*(t_j)\right\rangle = \frac{1}{Z[0,0]}\prod_{i=1}^{m}\prod_{j=1}^{n}\frac{\delta}{\delta\tilde{J}(t_i)} \times \frac{\delta}{\delta J(t_j)}Z[J,\tilde{J}] \tag{A4}$$

which is approximated as a sum of diagrams with m incoming and n outgoing arrows. Therefore, we can intuitively derive diagrams that connect the terms, either for the characteristic functional or for the cumulant generating functional $W[J,\tilde{J}]$, which are easier to derive since only diagrams that connect all the nodes survive (Lera 2018). For example, for the first cumulant or mean of bed-load transport in Eq. (13), we sum the first three diagrams of the expansion with only one outgoing arrow, combining the diagrams in Eqs. (A1), (A2), and (A3). To calculate the numerical value of the moment approximation, each time integration is multiplied by a symmetry factor due to the number of repeated diagrams that appear in the expansion (Chow and Buice 2015), which corresponds to the number of ways arrows can be rearranged in each node of the diagram. The second and third diagrams in Eq. (13) have been multiplied by 2, since we have two ways of exchanging the incoming arrows in the same diagram. For

the case of the second cumulant or variance in equation 16, we sum all connected diagrams with 2 outgoing arrows, where the number of nodes equal to the order of the term in the expansion.

Acknowledgements This work has been supported by projects Fondecyt 1191785 and Fondecyt 11191077. We acknowledge the additional support from ANID/Fondap Grant 15110017 and the supercomputing infrastructure of the NLHPC (ECM-02). C.G. acknowledges fundings from Grant EAR-1734752 and Grant Conicyt-21120939.

Author contributions C.E. conceived the study. C.G. developed the numerical code and performed the 3D simulations. C.E., C.G., M.E.W., and W.B. analyzed the data, interpreted the results, and wrote the paper,

Funding The authors have not disclosed any funding.

Declarations

Conflict of interest The authors declare that they have no conflict of interest.

References

Adrian RJ (2007) Hairpin vortex organization in wall turbulence. Phys Fluids 19(4):041,301. https://doi.org/10.1063/1.2717527

Ancey C, Pascal I (2020) Estimating mean bedload transport rates and their uncertainty. J Geophys Res Earth Surf 125:e2020JF005,534. https://doi.org/10.1029/2020JF005534

Ancey C, Bohorquez P, Heyman J (2015) Stochastic interpretation of the advection–diffusion equation and its relevance to bed load transport. J Geophys Res Earth Surf 120(12):2529–2551. https://doi.org/10.1002/2014JF003421

Bagnold RA (1956) The flow of cohesionless grains in fluids. Philos Trans R Soc Lond A 225:49–63. https://doi.org/10.1098/rsta.1956.0020

Barnhart KR, Tucker GE, Doty S et al (2020) Inverting topography for landscape evolution model process representation: part 3, determining parameter ranges for select mature geomorphic transport laws and connecting changes in fluvial erodibility to changes in climate. J Geophys Res Earth Surf. https://doi.org/10.1029/2019JF005287

Bertin S, Friedrich H (2018) Effect of surface texture and structure on the development of stable fluvial armors. Geomorphology 306:64–79. https://doi.org/10.1016/j.geomorph.2018.01.013

Bressloff PC (2014) Stochastic processes in cell biology, vol 41. Springer, Berlin

Buice MA, Cowan JD (2007) Field-theoretic approach to fluctuation effects in neural networks. Phys Rev E 75(5):051,919. https://doi.org/10.1103/PhysRevE.75.051919

Cameron S, Nikora V, Witz M (2020) Entrainment of sediment particles by very large-scale motions. J Fluid Mech 888:A7. https://doi.org/10.1017/jfm.2020.24

Chow CC, Buice MA (2015) Path integral methods for stochastic differential equations. J Math Neurosci 5(1):8. https://doi.org/10.1186/s13408-015-0018-5

Church M (2006) Bed material transport and the morphology of alluvial river channels. Annu Rev Earth Planet Sci 34:325–354. https://doi.org/10.1146/annurev.earth.33.092203.122721

Church M (2007) Multiple scales in rivers. In: Habersack H, Piégay H, Rinaldi M (eds) Gravel-bed rivers VI: from process understanding to river restoration, developments in earth surface processes, vol 11. Elsevier, Amsterdam, pp 3–28. https://doi.org/10.1016/S0928-2025(07)11111-1

Drake TG, Shreve RL, Dietrich WE et al (1988) Bedload transport of fine gravel observed by motion-picture photography. J Fluid Mech 192:193–217

Einstein HA (1937) Der geschiebetrieb als wahrscheinlichkeitsproblem. PhD thesis, Swiss Federal Institute of Technology, Zurich, Switzerland

Einstein HA (1950) The bed-load function for sediment transportation in open channels. Technical Bull. 1026, USDA Soil Conservation Service, Washington, D.C

Escauriaza C, Sotiropoulos F (2009) Trapping and sedimentation of inertial particles in three-dimensional flows in a cylindrical container with exactly counter-rotating lids. J Fluid Mech 641:169. https://doi.org/10.1017/S0022112009991534

Escauriaza C, Sotiropoulos F (2011) Initial stages of erosion and bed form development in a turbulent flow around a cylindrical pier. J Geophys Res Earth Surf. https://doi.org/10.1029/2010JF001749

Escauriaza C, Sotiropoulos F (2011) Lagrangian model of bed-load transport in turbulent junction flows. J Fluid Mech 666:36–76. https://doi.org/10.1017/S0022112010004192

Escauriaza C, Paola C, Voller VR (2017) Computational models of flow, sediment transport and morphodynamics in rivers. In: Gravel-bed rivers: process and disasters, pp 1–31

Fan N, Singh A, Guala M et al (2016) Exploring a semimechanistic episodic Langevin model for bed load transport: emergence of normal and anomalous advection and diffusion regimes. Water Resour Res 52(4):2789–2801. https://doi.org/10.1002/2015WR018023

Ferdowsi B, Ortiz CP, Houssais M et al (2017) River-bed armouring as a granular segregation phenomenon. Nat Commun 8(1):1–10. https://doi.org/10.1038/s41467-017-01681-3

Feynman RP, Hibbs AR (1965) Quantum mechanics and path integrals. McGraw-Hill, New York

Frey P, Church M (2009) How river beds move. Science 325(5947):1509–1510. https://doi.org/10.1126/science.1178516

Furbish DJ, Haff PK, Roseberry JC et al (2012) A probabilistic description of the bed load sediment flux: 1. J Geophys Res Earth Surf, Theory. https://doi.org/10.1029/2012JF002352

Ganti V, Lamb MP, McElroy B (2014) Quantitative bounds on morphodynamics and implications for reading the sedimentary record. Nat Commun 5(1):1–7. https://doi.org/10.1038/ncomms4298

Gardiner C (2009) Stochastic methods: a handbook for the natural and social sciences, 4th edn. Springer, Berlin

Ghilardi T, Franca MJ, Schleiss AJ (2014) Bed load fluctuations in a steep channel. Water Resour Res 50(8):6557–6576. https://doi.org/10.1002/2013WR014449

Gilbert GK (1914) The transportation of debris by running water, vol 86. US Government Printing Office

González C, Richter DH, Bolster D et al (2017) Characterization of bedload intermittency near the threshold of motion using a Lagrangian sediment transport model. Environ Fluid Mech 17:111–137. https://doi.org/10.1007/s10652-016-9476-x

Guala M, Singh A, BadHeartBull N et al (2014) Spectral description of migrating bed forms and sediment transport. J Geophys Res Earth Surf 119(2):123–137. https://doi.org/10.1002/2013JF002759

Hassan MA, Reid I (1990) The influence of microform bed roughness elements on flow and sediment transport in gravel bed rivers. Earth Surf Process Landf 15(8):739–750. https://doi.org/10.1002/esp.3290150807

Herbut I (2007) A modern approach to critical phenomena. Cambridge University Press, Cambridge

Heyman J, Mettra F, Ma H et al (2013) Statistics of bedload transport over steep slopes: separation of time scales and collective motion. Geophys Res Lett 40(1):128–133. https://doi.org/10.1029/2012GL054280

Houssais M, Ortiz CP, Durian DJ et al (2015) Onset of sediment transport is a continuous transition driven by fluid shear and granular creep. Nat Commun 6(1):1–8. https://doi.org/10.1038/ncomms7527

Hristopulos D, Christakos G (1999) Renormalization group analysis of permeability upscaling. Stoch Environ Res Risk Assess 13(1):131–161. https://doi.org/10.1007/s004770050036

Huang CH, Tsai CW, Mousavi SM (2021) Quantification of probabilistic concentrations for mixed-size sediment particles in open channel flow. Stoch Environ Res Risk Assess 35(2):419–435. https://doi.org/10.1007/s00477-020-01886-x

Hunt JCR, Wray AA, Moin P (1988) Eddies, stream, and convergence zones in turbulent flows. In: Proceedings of the summer program. Center for Turbulence Research, NASA Ames/Stanford Univ., pp 193–208

Jerolmack DJ, Paola C (2010) Shredding of environmental signals by sediment transport. Geophys Res Lett. https://doi.org/10.1029/2010GL044638

Khosronejad A, Sotiropoulos F (2014) Numerical simulation of sand waves in a turbulent open channel flow. J Fluid Mech 753:150–216. https://doi.org/10.1017/jfm.2014.335

Kirby E, Whipple KX (2012) Expression of active tectonics in erosional landscapes. J Struct Geol 44:54–75. https://doi.org/10.1016/j.jsg.2012.07.009

Kristensen NR, Madsen H (2003) Continuous time stochastic modelling CTSM 2.3. Technical University of Denmark

Kristensen NR, Madsen H, Jørgensen SB (2004) Parameter estimation in stochastic grey-box models. Automatica 40(2):225–237. https://doi.org/10.1016/j.automatica.2003.10.001

Leary KCP, Schmeeckle MW (2017) The importance of splat events to the spatiotemporal structure of near-bed fluid velocity and bed load motion over bed forms: laboratory experiments downstream of a backward facing step. J Geophys Res Earth Surf 122(12):2411–2430. https://doi.org/10.1002/2016JF004072

Lee DB, Jerolmack D (2018) Determining the scales of collective entrainment in collision-driven bed load. Earth Surf Dyn 6(4):1089–1099. https://doi.org/10.5194/esurf-6-1089-2018

Lera S (2018) Constrained stochastic processes in complex socio-economic systems. PhD thesis, Swiss Federal Institute of Technology, Zurich, Switzerland

Ma H, Heyman J, Fu X et al (2014) Bed load transport over a broad range of timescales: determination of three regimes of fluctuations. J Geophys Res Earth Surf 119(12):2653–2673. https://doi.org/10.1002/2014JF003308

Man C, Tsai CW (2007) Stochastic partial differential equation-based model for suspended sediment transport in surface water flows. J Eng Mech 133(4):422–430. https://doi.org/10.1061/(ASCE)0733-9399(2007)133:4(422)

Marusic I, Adrian R (2013) The eddies and scales of wall turbulence. In: Davidson PA, Kaneda Y, Sreenivasan KR (eds) Ten chapters in turbulence. Cambridge University Press, Cambridge, pp 176–220

Masteller CC, Finnegan NJ (2017) Interplay between grain protrusion and sediment entrainment in an experimental flume. J Geophys Res Earth Surf 122(1):274–289. https://doi.org/10.1002/2016JF003943

McComb WD (2004) Renormalization methods: a guide for beginners. Oxford University Press, Oxford

Murray AB, Lazarus E, Ashton A et al (2009) Geomorphology, complexity, and the emerging science of the Earth's surface. Geomorphology 103(3):496–505. https://doi.org/10.1016/j.geomorph.2008.08.013

Oh J, Tsai CW (2018) A stochastic multivariate framework for modeling movement of discrete sediment particles in open channel flows. Stoch Environ Res Risk Assess 32(2):385–399. https://doi.org/10.1007/s00477-017-1410-3

Paola C (2016) A mind of their own: recent advances in autogenic dynamics in rivers and deltas. In: Autogenic dynamics and self-organization in sedimentary systems. SEPM Society for Sedimentary Geology. https://doi.org/10.2110/sepmsp.106.04

Papanicolaou A, Tsakiris AG, Wyssmann MA et al (2018) Boulder array effects on bedload pulses and depositional patches. J Geophys Res Earth Surf 123(11):2925–2953. https://doi.org/10.1029/2018JF004753

Pierce JK, Hassan MA (2020) Back to Einstein: burial-induced three-range diffusion in fluvial sediment transport. Geophys Res Lett 47(15):e2020GL087,440. https://doi.org/10.1029/2020GL087440

Pledger AG, Rice SP, Millett J (2014) Reduced bed material stability and increased bedload transport caused by foraging fish: a flume study with juvenile Barbel (Barbus barbus). Earth Surf Process Landf 39(11):1500–1513. https://doi.org/10.1002/esp.3592

Radice A, Nikora V, Campagnol J et al (2013) Active interactions between turbulence and bed load: conceptual picture and experimental evidence. Water Resour Res 49(1):90–99. https://doi.org/10.1029/2012WR012255

Ravazzolo D, Mao L, Escauriaza C et al (2019) Rusty river: effects of tufa precipitation on sediment entrainment in the Estero Morales in the central Chilean Andes. Sci Total Environ 652:822–835. https://doi.org/10.1016/j.scitotenv.2018.10.287

Rößler A (2010) Runge–Kutta methods for the strong approximation of solutions of stochastic differential equations. SIAM J Numer Anal 48(3):922–952. https://doi.org/10.1137/09076636X

Saleur H, Sammis CG, Sornette D (1996) Discrete scale invariance, complex fractal dimensions, and log-periodic fluctuations in seismicity. J Geophys Res Solid Earth 101(B8):17661–17677. https://doi.org/10.1029/96JB00876

Särkkä S, Solin A (2019) Applied stochastic differential equations, vol 10. Cambridge University Press, Cambridge

Schmeeckle MW (2014) Numerical simulation of turbulence and sediment transport of medium sand. J Geophys Res Earth Surf 119(6):1240–1262. https://doi.org/10.1002/2013JF002911

Séchet P, Le Guennec B (1999) Bursting phenomenon and incipient motion of solid particles in bed-load transport. J Hydraul Res 37(5):683–696. https://doi.org/10.1080/00221689909498523

Shih W, Diplas P (2018) A unified approach to bed load transport description over a wide range of flow conditions via the use of conditional data treatment. Water Resour Res 54(5):3490–3509

Smits AJ, McKeon BJ, Marusic I (2011) High-Reynolds number wall turbulence. Annu Rev Fluid Mech. https://doi.org/10.1146/annurev-fluid-122109-160753

Sornette D (2006) Critical phenomena in natural sciences. Chaos, fractals, selforganization and disorder: concepts and tools. Springer, Berlin

Tsai CW, Huang SH (2019) Modeling suspended sediment transport under influence of turbulence ejection and sweep events. Water Resour Res 55(7):5379–5393. https://doi.org/10.1029/2018WR023493

Tsai CW, Hung SY, Oh J (2018) A stochastic framework for modeling random-sized batch arrivals of sediment particles into open channel flows. Stoch Environ Res Risk Assess 32(7):1939–1954. https://doi.org/10.1007/s00477-018-1529-x

Tsai CW, Hung SY, Wu TH (2020) Stochastic sediment transport: anomalous diffusions and random movement. Stoch Environ Res Risk Assess 34(2):397–413. https://doi.org/10.1007/s00477-020-01775-3

Vignaga E, Sloan DM, Luo X et al (2013) Erosion of biofilm-bound fluvial sediments. Nat Geosci 6(9):770–774. https://doi.org/10.1038/ngeo1891

Werner B (1999) Complexity in natural landform patterns. Science 284(5411):102–104. https://doi.org/10.1126/science.284.5411.102

Wohl E (2019) Forgotten legacies: understanding and mitigating historical human alterations of river corridors. Water Resour Res 55(7):5181–5201. https://doi.org/10.1029/2018WR024433

Yang JQ, Nepf HM (2019) Impact of vegetation on bed load transport rate and bedform characteristics. Water Resour Res 55(7):6109–6124. https://doi.org/10.1029/2018WR024404